Mon. Not. R. astr. Soc. (1990) **244**, 408–423

The LDSS deep redshift survey

Matthew Colless,[1]★ Richard S. Ellis,[1] Keith Taylor[2] and Richard N. Hook[3]†

[1] *Physics Department, University of Durham*
[2] *Anglo-Australian Observatory, Epping, NSW, Australia*
[3] *Department of Physics and Astronomy, University College London*

Accepted 1989 December 6. Received 1989 November 14; in original form 1989 August 3

SUMMARY

Using a new multislit spectrograph, LDSS, we have obtained intermediate dispersion spectroscopy for a new sample of 149 faint objects selected randomly from the magnitude range $21 \leq b_J \leq 22.5$ in three high-latitude fields. Our overall success rate of 81 per cent for spectroscopic identification is comparable to that achieved in the earlier fibre survey of Broadhurst *et al.* to $b_J = 21.5$, demonstrating that LDSS has pushed the limiting magnitude for field surveys 1 mag deeper. Of identified objects, 28 per cent are galactic stars, in reasonable agreement with estimates based on image classification. The remaining objects are galaxies with redshifts $0 < z < 0.7$. Despite the 19 per cent incompleteness, the extended wavelength coverage and continuum signal-to-noise ratio of our spectra imply that the observed redshift distribution is representative of galaxies at these magnitudes, and that we can rule out a significant excess of high-redshift galaxies. At $b_J = 22.5$, the galaxy counts are approximately twice the no-evolution model prediction, yet we find the redshift distribution to be close to that expected for a non-evolving population. At least half the excess population must therefore have $z < 0.5$. The absence of *any* identified galaxies with $z > 0.7$ to $b_J = 22.5$ provides important constraints on models where galaxy luminosities evolve monotonically with redshift in a luminosity-independent way. In particular, we can place new limits on the evolution of luminous galaxies since $z \sim 1.5$–2. Our data support earlier suggestions that the steep slope of the number–magnitude counts is mostly due to the evolution of galaxies at the faint end of the galaxy luminosity function. We also find a significant excess over non-evolving models in the proportion of galaxies with strong [O II] 3727 Å emission, indicating that star formation is more common at these faint magnitudes. The implications of our spectra for a proposed population of high-redshift flat-spectrum galaxies with high star-formation rates are also discussed.

1 INTRODUCTION

Recent advances in multiple object spectroscopy on 4-m class telescopes have transformed not only statistical projects on objects of moderate and intermediate brightness (e.g. Colless & Hewett 1987; Sharples, Ellis & Gray 1988), but also have encouraged work at faint limits ($B \leq 21.5$), where the multiplex gain justifies the long integrations required (e.g. Couch & Sharples 1987; Boyle *et al.* 1987; Broadhurst, Ellis & Shanks 1988).

The work cited above was carried out with the AAT's fibre-optic coupler FOCAP (Gray 1986), which provides adequate sky subtraction to these magnitude limits (Ellis 1987). However, in fainter regimes where sky subtraction is the limiting factor, the advantages of multislit aperture plates over fibre couplers have been demonstrated in studies of distant galaxy clusters (Dressler & Gunn 1982) and in another faint redshift survey in progress (Koo & Kron 1988; Koo 1988). Multislits nonetheless suffer the disadvantages of a much smaller multiplex gain (~ 15 *cf.* ~ 50) and a smaller field of view (~ 5 arcmin *cf.* ~ 40 arcmin) (Ellis & Parry 1988).

This has not hampered studies of clustered objects, but for field surveys fainter than $B \sim 21.5$ it was clear to two of us (KT and RSE) several years ago that a new dedicated wide-

★Present address: Institute of Astronomy, Madingley Road, Cambridge CB3 0HA.
†Present address: STECF, ESO, Karl Schwarzschild Str.-2 D-8046, FRG.

field instrument was required. This realization led to a specification for a new low dispersion survey spectrograph (LDSS), with the principal aim of combining the multiplex gain of fibre optics with the sky subtraction gain of multislits at faint limits. The major advance was a novel optical design by Wynne & Worswick (1988) offering a 12.3 arcmin diameter field with imaging performance <1 arcsec FWHM. The resulting instrument was constructed jointly by Durham University and the Royal Greenwich Observatory and commissioned on the AAT during 1985 and 1986.

Since the pioneering deep photographic surveys of the 1970s (e.g. Kron 1978; Peterson *et al.* 1979; Tyson & Jarvis 1979) it has been realized that spectroscopy of statistically complete samples of faint galaxies is necessary for establishing the evolutionary history of galaxies, vital to their possible use as cosmological probes. Photometry alone, even when gathered across many passbands, cannot reliably provide redshift estimates for all classes of galaxies, or identify new populations that might be present at faint limits.

A fundamental question posed by the deep surveys concerns the steep slope of the number–magnitude counts. This has often been used as evidence for luminosity evolution in normal galaxies from $z\sim2$ to the present epoch. From a comprehensive survey of over 200 faint galaxies using the AAT fibre coupler, Broadhurst, Ellis & Shanks (1988; hereafter BES) showed that the observed redshift distribution $n(z)$ at $b_J\sim21.5$ (where $b_J\equiv$ Kodak IIIa-J + GG385) allowed evolution only in *low luminosity* galaxies. They tentatively identified the excess population of faint galaxies with a new population of star-forming galaxies and presented a model whereby short-lived bursts of star formation temporarily brighten otherwise low-luminosity systems. If correct, this explanation might have significant implications for the very faint blue galaxies being found in CCD extensions of the original photographic surveys (Tyson 1988; Cowie 1988), suggesting that many are not high redshift primevals, but rather intermediate luminosity galaxies at modest redshift.

At the fibre coupler limit the excess number of galxies (over and above the no-evolution expectation) is only ~30 per cent, and it is premature to generalize BES' explanation of the steep counts slope at $b_J\sim21.5$ to that seen at much fainter limits. However, the fractional excess rises steeply with increasing limiting magnitude, so that a deeper survey provides an important test for this hypothesis. This paper presents a spectroscopic survey of a randomly selected sample of stars and galaxies in the magnitude range $21.0\leq b_J\leq22.5$, extending BES' earlier survey work by one magnitude. Some preliminary results from this survey were reported by Colless *et al.* (1988), and their similarity to those provisionally derived from an independent northern deep survey (Koo & Kron 1988) has been remarked by Koo (1988).

The paper is organized as follows. Section 2 describes the essential features of LDSS, including the techniques developed for multislit fabrication and for acquiring fields at the telescope. Some instrumental performance estimates are also given. In Section 3 we review briefly what is known about populations of objects fainter than earlier surveys (i.e. $B\approx21.5$), and discuss the selection strategy for this survey. We present the spectroscopic observations in Section 4 along with a discussion of the data reduction techniques. The resulting galaxy redshift distribution, and its completeness, are analysed in Section 5. The results are discussed with respect to our understanding of galaxy evolution in Section 6. Our principal conclusions are summarized in Section 7.

2 THE LOW DISPERSION SURVEY SPECTROGRAPH

The main considerations driving the optical design of the low dispersion survey spectrograph (LDSS) were high efficiency and a wide field of view with good image quality. For a multislit spectrograph the widest possible field allows the largest possible multiplex gains, and is essential in obtaining a significant multiplex advantage when studying rarer types of objects. Wynne & Worswick (1988) have described the novel optical design of LDSS, which leads to a 12.3 arcmin diameter field. At the $f/8$ Cassegrain focus of the AAT, the image scale on the multislit aperture mask is 6.7 arcsec mm^{-1}, while at the focus of the $f/2$ camera it is 26.3 arcsec mm^{-1}.

In order to maximize efficiency, LDSS uses lenses throughout, then employs a transmission grating (grism) as the dispersing element. The complexity of the lens system requires the use of effective multilayer anti-reflection coatings in order to maintain a high throughput. To avoid an overlapping second order, and since the anti-reflection coatings are only effective over an octave of wavelength, the design was tuned for the spectral range 3700–7500 Å. This blue wavelength range was chosen because a principal scientific goal was the investigation of the steep slope of the number–magnitude counts, for which the excess is greatest in the *U*- and *K*-bands (Koo 1981). A deeper limit in terms of this excess can be reached, for a given sky-subtraction precision (as a fraction of sky), at blue-to-visual wavelengths, where the sky spectrum is relatively smooth. Over the whole wavelength range the FWHM of the PSF is better than 35 μm (i.e. <1 arcsec) across the full field. Two grisms, having dispersions of 165 and 870 Å mm^{-1}, are currently available. The optical throughput of LDSS at 5500 Å is as follows: collimator and camera alone, 80 per cent; optical train including 165 Å mm^{-1} grism, 60 per cent; entire system including zenith atmosphere, telescope and RCA CCD, 34 per cent. The IPCS used in this survey has a quantum efficiency ~3 times lower than the RCA CCD at 5500 Å, but this is more than compensated for by its extremely large detector area, vital for intermediate dispersion spectra over a wide field, and zero read-noise. Scattered light and ghosts from optical reflections are limited to <0.2 per cent, an important factor for faint object work. Further details of the design are given by Wynne & Worswick.

The focal reducer design of LDSS permits four different modes of operation.

(i) Direct mode. Removing the grism, LDSS can be used as a simple $f/2$ focal reducer for obtaining direct broad- or narrow-band images. In 1 arcsec seeing the FWHM spatial resolution is ~50 μm (1.3 arcsec), which is well matched to typical detector pixel sizes of 20–30 μm. Although more coarsely sampling the sky, the direct imaging mode has a wider field of view and, in the case of the mean AAT seeing (~1.5 arcsec), is approximately twice as fast as an equivalent $f/3$ prime focus. This mode can be used for obtaining photo-

metry/astrometry of deep spectroscopic targets, for field acquisition, and for calibration purposes.

(ii) Long slit mode. Long slit aperture masks can be made for any desired slit width. A slit of width 1.7 arcsec gives FWHM spectral resolutions of ~13 and ~70 Å at 160 and 870 Å mm^{-1}, respectively.

(iii) Slitless mode. With no aperture mask, spectra of all objects in the field may be obtained simultaneously, though overlaps and sky contamination reduce the performance. The resolution is also seriously degraded if the seeing is worse than about 2 arcsec.

(iv) Multislit mode. This is the primary mode of LDSS as a survey spectrograph. Using an aperture mask with slits 10–25 arcsec in length, between 20 and 100 targets (depending on the dispersion and the detector) may be observed simultaneously.

The design of multislit masks from a target catalogue giving precise astrometric positions is a complex process, which is greatly aided by the LEXT software package designed purposely for use with LDSS. LEXT enforces various important observational constraints on the mask design, and also permits interactive optimization of the design to achieve the maximum multiplex advantage under a user-specified set of priorities for the target objects. The enforceable constraints (and their adopted values in this survey) are: (i) a minimum slit length, to ensure accurate sky subtraction (15 arcsec); (ii) a minimum distance from objects to the ends of their slits, so that sky can be interpolated across an object (5 arcsec); (iii) a range of position angle, so that the effects of atmospheric dispersion are minimized for the planned span of hour angles; (iv) the spectral range which must be free of overlap with neighbouring spectra (3700–7500 Å); (v) a minimum separation between the ends of neighbouring slits, also to prevent overlaps (1 arcsec); (vi) whether or not zero orders may fall on the sky region of other spectra (permitted).

The degrees of freedom allowed in the optimization process are the length of the slit, the position of the object with respect to the centre of its slit and the position angle for the observation. Fully automatic optimization, under the above constraints, of the number of objects observed, weighted by their respective priorities, is very difficult. We take a pragmatic and interactive approach, first restricting the number of free parameters by fixing the position angle to a value appropriate to observing the field symmetrically about the meridian. LEXT then employs a detailed model of the imaging and spectral performance of LDSS to predict the dispositions on the mask of all the spectra in the target catalogue. These are then eliminated in reverse order of priority until all the constraints are satisfied. This process is carried out with the aid of interactive graphics in the case of equal priorities. Finally, the mask design for the remaining targets is further enhanced by maximizing the slit lengths while still enforcing the various constraints.

Once a satisfactory design has been agreed, the mask is drawn on a high-precision plotter at twice-actual scale and with calibration marks for establishing orientation and scaling. This blueprint is then used by a commercial manufacturer to photochemically etch the slits in a steel template. The mask thus produced has slit edges with a separation that is constant at a level of <0.5 per cent on a 50 μm (about a resolution element) scale, as is necessary for sky subtraction at these magnitudes.

Several methods for acquiring a field through a multislit mask have been developed. The one employed in these observations, which is well-suited to the limited imaging capabilities of the imaging photon counting system (IPCS) on the AAT, employs three or more fiducial stars. These are added to the target catalogue with the highest priority, ensuring that they are included in the mask design. Instead of slits, however, circular apertures 10 arcsec in diameter are etched for these fiducials in the mask. At the telescope, field acquisition then proceeds as follows. The pointing accuracy of the AAT is sufficiently good to blindly acquire the fiducial stars down their apertures. Further tuning of the translational and rotational positioning is then carried out by imaging the relative positions of the stars with respect to their aperture centroids. This relatively complex procedure is carried out by a LEXT routine which takes two direct images as input (taken through the mask) of the field and a white light source, and outputs offsets for the AAT guide probe. Using this method, precision field acquisition can be achieved in less than 10 min.

3 SURVEY STRATEGY AND SAMPLE SELECTION

Deep photographic and CCD photometry of galaxies shows that the number of counts of galaxies in the blue have a much steeper slope than can be accounted for without some form of evolution (Hall & Mackay 1984; Shank *et al.* 1984). Over the range $18<b_J<25$, the observed number counts are closely log-linear, and have slope 0.45 ± 0.02 (Metcalfe *et al.* 1987; Tyson 1988; Jones *et al.*, in preparation). In comparison, models for the number counts using the local properties of the galaxy population and assuming no evolution yield slopes in the range 0.3–0.35. If the observed counts are assumed to be very close to the no-evolution model at $b_J=18$, this difference in slopes would imply that the observed numbers of galaxies at $b_J=20$, 22 and 24 are in excess of the model by factors of 1.6, 2.5 and 4, respectively. Faint number counts in the U passband (Majewski 1988) have an even steeper slope, and thereby exceed no-evolution predictions by a greater amount, while those in R and I (Tyson 1988) are flatter and close to the no-evolution model.

Various hypotheses have been advanced to account for this excess in the number counts. Kron (1982) has pointed out that the uncertainties in the local space density of blue, low-luminosity galaxies allow one to account for the excess without invoking evolution, since they suffer little redshift dimming and therefore constitute an increasing fraction of the total galaxy population at fainter magnitudes. Alternatively, the counts may be adequately fitted by simple models involving a monotonic brightening with increasing redshift of the entire galaxy luminosity function. These models assume either that all galaxies have the same luminosity evolution (Shanks *et al.* 1984) or that the luminosity evolution depends only on morphological type and not on luminosity (Peterson *et al.* 1979; Koo 1986). There is also the possibility that at least some fraction of the count excess is composed of primeval galaxies at high redshift undergoing their first strong burst of star formation.

The most direct way to test these and other plausible hypotheses is to obtain the redshift distribution of galaxies in faint magnitude-limited samples. If the count excess is produced by a previously underestimated population of dwarf galaxies, the distribution will have a larger low-redshift tail than predicted by the no-evolution model. If, on the other hand, general luminosity evolution or a population of primeval galaxies is responsible for the excess, there will be a large high-redshift tail.

An important step in this direction has been taken by BES who found, contrary to the earlier expectations based on photometry alone (e.g. Koo 1981, Ellis 1982), that the redshift distribution for a complete magnitude-limited sample showed neither a high nor a low tail when compared to the no-evolution model. To simultaneously explain the steep number count slope whilst maintaining the no-evolution redshift distribution, BES suggested a model in which only the faint end of the luminosity function evolves over recent times. From spectral properties of their sample, BES postulated that short-lived bursts of star formation in this low-luminosity population would brighten them temporarily.

The main aim of the present survey is to obtain the galaxy redshift distribution to the faintest possible limiting magnitude in order to place (in conjunction with the number counts) the strictest possible constraints on galaxy evolution. The limiting magnitude of the survey was defined by the performance of LDSS to be $b_J = 22.5$, one magnitude deeper than the previous deepest survey by BES. Simulations based on the measured throughput of the instrument at 5500 Å showed that at 13 Å resolution a mean sky subtracted continuum signal-to-noise ratio >4–5 could be achieved with useful slit lengths (~ 15 arcsec) in half a night.

The survey samples were randomly drawn from photometric catalogues constructed from COSMOS (MacGillivray & Stobie 1984) scans of deep AAT prime focus plates. Experiments with star/galaxy separation both by eye and using the COSMOS image classification software implied that, at this magnitude limit, the fractions of stars misclassified as galaxies, and galaxies as stars, were both greater than 10 per cent. It was considered that this rate of misclassification (which was subsequently confirmed spectroscopically – see below) might lead to a significant morphological bias in the survey samples, and so the COSMOS image classification was ignored – both stars and galaxies were therefore included in the survey. At these magnitudes stars comprise less than 30 per cent of the total number of objects, so that their inclusion results in only a small decrease in the efficiency of the survey as far as galaxies are concerned.

All the zones of the spectral survey have both b_J and r_F (where $r_F \equiv$ Kodak IIIa-F + Schott RG630) photographic photometry. The deep AAT prime focus plates on which this photometry was based are listed in Table 1 and were obtained originally for an extensive investigation of the variation in the number–magnitude counts from field to field (Jones *et al.*, in preparation). The COSMOS magnitudes are isophotal, with thresholds of 26.4–26.7 mag arcsec^{-2} in b_J and 24.6–25.2 mag arcsec^{-2} in r_F (see Table 1). The different thresholds introduce systematic errors in the galaxy magnitudes of 0.13 mag at $b_J = 22.5$ and 0.15 mag at $r_F = 21.5$ and less for the stars. However, most of this difference is removed by calibrating each plate independently to CCD total magnitudes.

The CCD observations and reduction techniques are discussed in detail by Jones *et al.* and (for the SGP) by Couch, Shanks & Pence (1985). Standard sequences of stars and galaxies to $b_J = 23.5$ and $r_F = 21.5$ were measured with large (>10 arcsec diameter) apertures to obtain total magnitudes. Separate calibrations were determined for stars and galaxies according to the procedure given in Shanks *et al.* (1984). Although this pre-judges their spectral classifications, in practice the difference at the survey limit is ≤ 0.05 mag. The standard errors in the zeropoints, estimated from the scatter on the COSMOS–CCD calibration curves, were typically 0.05 mag for $b_J < 23$ and $r_F < 21$. The b_J zeropoints for the 10 and 13 hr fields agree with the independent CCD calibrations of Stevenson *et al.* (1985) and Boyle (1986) for corresponding UK Schmidt Telescope plates, which apply brighter than 20.5 mag.

Further CCD observations carried out by MMC using the KPNO No. 1 0.9-m telescope on 1988 January 14 indicate that the zeropoint errors for the 10 hr field are ≤ 0.05 mag in b_J and ≤ 0.12 mag in $b_J - r_F$ to the full depth of the survey. We have also checked the relative precision of the COSMOS photometry via CCD photometry obtained by L. Miller and K. Glazebrook with the Isaac Newton Telescope on La Palma during 1988 April. This photometry is part of an ongoing series of observations intended to provide accurate CCD photometry for all survey fields. The CCD images lie in the survey zones 10.2 and 13.2, but only cover a fraction of the full LDSS zone in each case. Moreover, shutter problems during the observing run prevent reliable zeropoints being derived. We have therefore used this photometry only to estimate the precision of the photographic photometry obtained with COSMOS. The image analysis and photometry of the CCD data were performed with a modified version of the GALAXY software package (Godwin 1976). Fig.

Table 1. Photographic plate material.

(1) Field	(2) α (1950)	(3) δ (1950)	(4) Plates	(5) Isophote (mag arcsec^{-2})	(6) Survey magnitude range
00 hr	00 54 48.1	−27 54 45	J1888	26.72	$20.92 \leq b_J \leq 22.71$
(SGP)	00 54 48.7	−27 54 04	F1996	25.20	
10 hr	10 43 37.9	−00 04 48	J1834	26.44	$20.98 \leq b_J \leq 22.48$
	10 43 37.9	−00 04 48	F1835	24.61	
13 hr	13 41 14.0	−00 00 29	J1836	26.52	$21.00 \leq b_J \leq 22.44$
	13 41 14.0	−00 00 29	F1837	24.82	

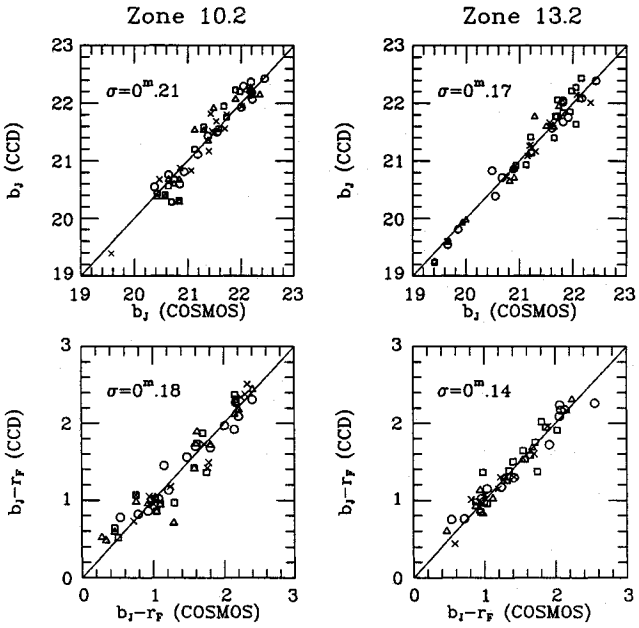

Figure 1. A comparison of the COSMOS photographic photometry used in this survey with CCD photometry in two LDSS zones. The various symbols on each plot refer to different CCD fields in each zone. Standard deviations about the mean are indicated.

1 shows the comparison between the CCD and COSMOS photometry for the images common to both sets of data. The zeropoints for the CCD photometry have been defined so as to give zero mean offset with respect to the COSMOS photometry. Standard deviations about the mean are indicated in the figure. For b_J and $b_J - r_F$ these are ≤ 0.2 mag in both zones, giving us considerable confidence in the photographic photometry in these bands.

For each LDSS zone (a region of 5.3×12.3 arcmin), the objects to be surveyed were randomly selected over the range $21.0 \leq b_J \leq 22.5$ from the photometric catalogue for that field. However, because Jones *et al.*'s final photometric calibration only became available after the observations were made, small adjustments to the zeropoints mean that the actual selection ranges vary slightly from the nominal range (see Table 1). (Note that this new calibration also applies to the magnitudes in BES' SGP field, which should be 0.21 mag fainter than their published values.) That the selected objects are a magnitude-unbiased fair sample of the photometric catalogue for each field was confirmed by comparing the cumulative number–magnitude distributions. Kolmogorov–Smirnov (K–S) tests showed that the magnitude distributions of the spectroscopic samples did not differ in any case from those in the corresponding catalogue at the 10 per cent confidence level. Applying a similar test shows that the $b_J - r_F$ colour distribution of the selected sample is also representative of the entire COSMOS catalogue given our b_J limits. This is important since we shall later correlate colour and spectral line diagnostics with redshift to address the implications of the survey for fainter samples.

The only bias introduced in this selection procedure is due to the geometrical constraints on how close two slits may be placed in order to avoid overlapping spectra. As described in Section 2 above, the enforced minimum slit length and minimum distance between the object and the end of the slit, together with the actual placement of the object along the slit, determine the size and position of the selected object's slit. This then defines an exclusion region about this object from which no further objects may be chosen. The Y extent of this region (typically ~ 15–20 arcsec) is that of the slit plus the small minimum separation between slits at either end. The X extent of this zone is the full 5.3 arcmin of the LDSS zone. Objects are chosen in sequence from one Y limit of the zone to the other so as to fit as many as possible on to a single mask.

This selection procedure leads to a mild tendency to sample the field at approximately 20 arcsec intervals in Y. Since the angular correlation function, $w(\theta)$, on scales of $\theta \sim 20$ arcsec is $\sim 0.2 \pm 0.1$ at $b_J \approx 22.5$ (Ellis 1980; Koo & Szalay 1984; Stevenson *et al.* 1985), the majority of excluded objects close to a chosen galaxy should not be physically associated with it. The selection procedure should not therefore significantly alter the effect of clustering in the measured redshift distribution. Nonetheless, it would be dangerous to use this catalogue for clustering analyses on small scales since 20 arcsec corresponds to $\sim 0.1\ h^{-1}$ Mpc at the mean redshift of the survey.

4 OBSERVATIONS AND DATA REDUCTION

A log of the spectroscopic observations with LDSS is given in Table 2. This lists the zone identifier and centre, the total integration time, the dates of the observations and the sampling rate of the survey in that zone. With the masks constructed as described in Section 2 according to the strategy in Section 3, the observing proceeded according to the requirement that all spectroscopic zones should receive about half a night's integration ($\sim 15\,000$ s). In practice, weather problems prevented such uniform treatment. Some zones were observed over more than one night, others received less than the desired integration. As we demonstrate below, the non-uniform integration times do not seriously affect the survey's field-to-field completeness.

To obtain fully reduced spectra from LDSS with the IPCS as detector, at least two types of calibration image are required.

(i) Direct images of a matrix mask using white light illumination. A matrix mask is simply a mask covered with small holes in a regular grid. These images are taken both at the start and at the end of the observations of the target field. They cannot be taken once the field has been acquired (see

Table 2. Details of spectroscopic survey.

(1) Survey Zone	(2) α (1950)	(3) δ (1950)	(4) Dates of observations	(5) Integration time (s)	(6) Sampling rate	(7) Completeness
00.2	00 54 49.4	−27 43 53	23,24/10/87	20000	0.36	80%
10.2	10 43 55.4	+00 05 33	19/3/88	13500	0.25	87%
10.4	10 43 51.4	−00 06 41	22/3/88	12000	0.23	82%
13.2	13 41 57.3	+00 06 25	19,23/3/88	18000	0.23	73%
13.4	13 41 09.1	−00 00 16	22/3/88	11500	0.24	87%
13.5	13 41 08.8	+00 10 18	21/3/88	15000	0.24	74%

Notes: (i) the survey zone is $f.z$, where f is the field R.A., and z is the zone number in that field; (ii) the sampling rate is $N(Q=1,2,3)/\langle N(21 \leq b_J \leq 22.5)\rangle$; (iii) the completenes is $N(Q=1,2)/N(Q=1,2,3)$.

Section 2) as the field would then need to be re-acquired. The matrix mask images are used to remove the distortions introduced across the field by the optics and the IPCS.

(ii) Calibration lamp spectra taken through the slit mask used for the observations. These wavelength calibration spectra are interleaved among the observations of the target field to provide checks on the stability of the spectrograph and detector.

The distortion of the images caused both by the optics and the magnetic focusing of the IPCS is severe, amounting to several pixels at the edge of the field. The matrix mask images allow this distortion to be mapped and removed by the LEXT software through a comparison of the predicted positions of the matrix gridpoints and the observed distorted image. To make this comparison, the predicted image must first be calculated from the known parameters of the precisely manufactured matrix mask. The mask grid is scaled to the predicted image at the detector using the known mask-to-detector focal reduction ratio and the measured IPCS pixel dimensions. The latter are derived from the essentially undistorted central 3×3 gridpoints of the observed matrix. The gridpoints in the observed and predicted image are then matched, and a bicubic spline transformation from undistorted to distorted coordinates is obtained by fitting between the matched grids. The residuals of the bicubic spline fit are typically ≤ 0.1 pixel. An undistorted image may then be formed by transforming each of its pixels into distorted coordinates and interpolating a pixel value from the distorted image. The adopted interpolation scheme employed a multilinear fractional-pixel algorithm with guaranteed flux conservation.

The major limitation of this technique for correcting distortion is that only that part of the image lying within the undispersed field of view is corrected. The parts of spectra falling outside this region are still strongly distorted. With the instrumental setup used here, the spectra fill about two-thirds the width of the detector, and so a significant amount of information at either end of the spectrum is lost for perhaps 20 per cent of the objects observed. The problem of distortion will be greatly reduced once the large-format CCDs, with which LDSS was designed to operate, become available.

This distortion map is computed for the matrix mask images taken both before and after the observations of a particular field in order to test that the distortion remained stable over this period. The distortion correction is then applied to each of the calibration arc images. Intercomparison of the corrected arcs provides a check on the stability of the distortion throughout the observing sequence. Once this stability is confirmed, the arc exposures, and the exposures of the target objects, may be co-added to give integrated arc and object images.

An individual wavelength calibration for each slit is then derived from the arc image. The helium arc used here gave calibrations with typical rms errors of 1–2 Å. The unresolved arc lines had a FWHM of 13 Å. The wavelength calibrations were independently checked using the sky spectra from each slit. Each sky spectrum was divided into seven 500 Å-long sections, which were cross-correlated with the corresponding sections of a template sky spectrum in order to find wavelength shifts. Excluding those parts of spectra lying outside the distortion-corrected region, no large shifts were found. The typical wavelength shift found in the sections covering the range 3800–6300 Å was 1.5–2.5 Å. The sections covering 6300–7300 Å showed typical shifts of 3–4 Å, or less than a third of a resolution element.

The extraction of the object spectra from the undistorted, co-added image proceeds as follows:

(i) The regions covered by each slit spectrum, referred to as 'boxes', are calculated. In Y this is the known spatial extent of the slit. The X extent is computed from an adopted approximate spectral range using the calibrated wavelength–pixel relation for the slit. The position of the object in the slit is also predicted from the information used to generate the slit mask.

(ii) The box is summed along its (spectral) X-axis and the resulting slit profile analysed to obtain an improved value for the position of the object and to estimate its extent along the slit. This region is excluded from consideration and the remaining points of the slit profile are filtered by σ-clipping about the median to remove secondary objects and other defects not related to the sky level. Finally, a low-order polynomial is fitted in order to give an estimate of the true slit profile. Sky subtraction proceeds by subtracting a normalized version of this profile from each column of the box. The normalization is determined by the sum over the pixels belonging to the rows included in determining the estimated profile. Sky subtraction using this procedure was typically accurate to 0.5 per cent, as measured from the rms residuals in the sky-subtracted sky spectrum (see Fig. 2).

(iii) To recover the spectrum with near-optimal signal-to-noise, the object is assumed to have an approximately Gaussian profile defined by the position and FWHM estimated during the sky subtraction process. (This assumption is quite adequate for the spatially under-sampled data dealt with here.) A weighted sum is performed in the spatial direction along each column in the box over the estimated extent of the object, with the assumed Gaussian profile providing the relative weights. The extracted spectrum is lastly wavelength-calibrated.

In fact, the box may, if desired, be divided along its spectral axis into smaller blocks for sky subtraction and extraction. This allows one to recover some information from the distorted parts of spectra. The entire reduction sequence, from removing the distortion through wavelength calibration, sky-subtraction and optimal extraction of the object spectrum, is carried out in a highly automated yet flexible fashion using the LEXT software.

Some examples of the spectra obtained in this survey are shown in Fig. 3. Relative flux calibration was performed using observations of the flux-standards GD190 and L970-30 (Oke 1974). Absorption features as well as emission lines can be found in objects up to the limiting magnitude of $b_J = 22.5$.

The survey redshift catalogue is presented in Table 3. Redshifts for the galaxies in the survey were obtained from visual identification of spectral features. If the [O II] 3727 Å emission line was present, the redshift was re-determined from a Gaussian fit to this feature. The redshifts have typical internal errors of 300–500 km s^{-1}, which is too small to have any effect on the results derived here. Each redshift has been assigned a quality class Q (column 8) as follows: (i) $Q = 1$: the

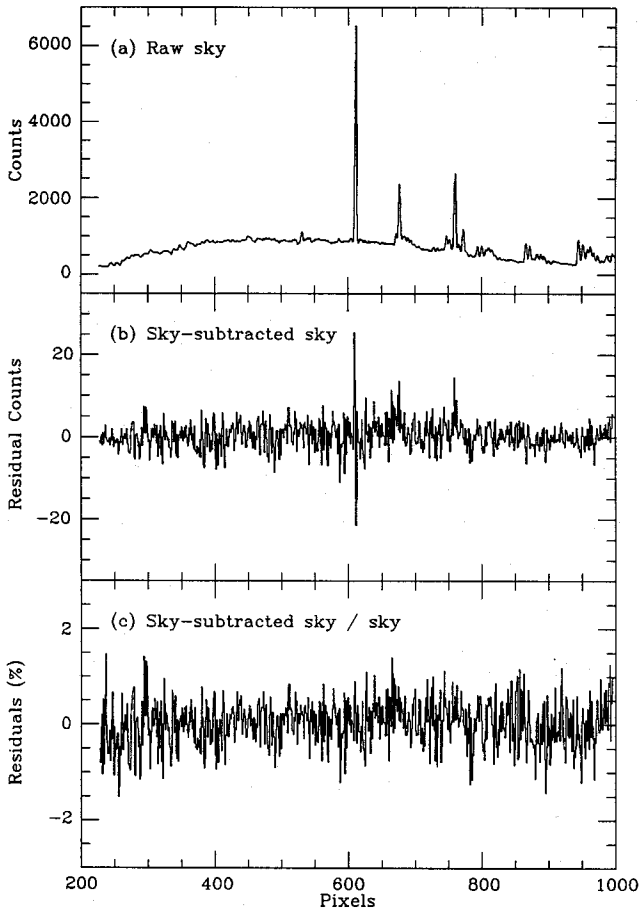

Figure 2. (a) An example of a raw sky spectrum. Note the strong night sky emission lines at 5577, 5892 and 6300 Å; (b) for the same slit, these are the residuals after the sky on one side of the object spectrum is subtracted from the sky on the other side using the techniques described in the text; (c) the sky subtracted sky residuals as a fraction of sky. Note that the large residuals apparent in the three sky lines in (b) are due only the strength of these lines and do not stand out in this plot.

most reliable redshifts, confirmed by more than one spectral feature; (ii) $Q=2$: redshifts based on a single feature (usually [O II] 3727 Å or Ca *H* and *K* for galaxies, Mg I *b* band for stars); (iii) $Q=3$: spectra for which no redshift could be ascertained; (iv) $Q=4$: spectra which were too distorted to extract; (v) $Q=5$: survey sample objects for which no spectrum could be detected. As in BES, the majority of single-line identifications are based on [O II] 3727 Å and, in the case of the sample at $b_J \leq 21.5$, co-added spectra of these objects revealed Balmer absorption lines consistent with this interpretation.

In keeping with our goal of making the object selection as simple as possible, we defined targets *solely* on the basis of their COSMOS b_J magnitude (rather than insisting on a joint detection in more than one passband). We therefore expect a

Table 3. The LDSS deep redshift survey catalogue.

(1) ID (*f.z.#*)	(2) α (1950)	(3) δ	(4) b_J	(5) b_J-r_F	(6) S/G	(7) z	(8) Q	(9) W_λ (Å)
00.2.01	00 55 09.14	−27 43 14.9	20.92	1.33	g	0.163	1	60
00.2.02	00 54 48.49	−27 44 50.9	21.09	—	s	0.165	1	27
00.2.03	00 54 55.84	−27 39 54.6	21.22	2.28	g	0.331	1	5
00.2.04	00 55 09.45	−27 41 18.9	21.24	1.79	g	—	3	—
00.2.05	00 54 56.58	−27 40 31.4	21.34	0.61	g	0.330	2	—
00.2.06	00 55 03.04	−27 44 23.8	21.37	1.20	s	0.000	1	—
00.2.07	00 54 41.65	−27 41 30.1	21.40	1.94	g	0.000	1	—
00.2.08	00 54 58.85	−27 47 39.0	21.48	0.78	g	0.318	1	26
00.2.09	00 54 52.13	−27 39 11.3	21.51	1.39	s	0.000	1	—
00.2.10	00 55 04.95	−27 46 55.8	21.53	1.05	s	0.000	1	—
00.2.11	00 54 55.10	−27 39 25.2	21.58	2.59	g	0.421	1	—
00.2.12	00 55 00.17	−27 40 47.9	21.62	1.02	g	0.113	2	17
00.2.13	00 54 54.03	−27 41 44.6	21.65	2.51	s	0.317	1	—
00.2.14	00 55 00.97	−27 49 42.2	21.73	1.05	g	—	4	—
00.2.15	00 54 41.71	−27 45 29.2	21.75	1.41	s	0.000	1	—
00.2.16	00 54 49.15	−27 41 55.4	21.78	1.85	g	0.439	2	8
00.2.17	00 54 48.47	−27 39 36.5	21.78	2.48	g	0.329	1	—
00.2.18	00 54 50.60	−27 48 27.2	21.79	—	g	0.000	5	—
00.2.19	00 54 53.12	−27 41 06.7	21.81	0.00	g	0.217	2	14

Table 3. — *continued*

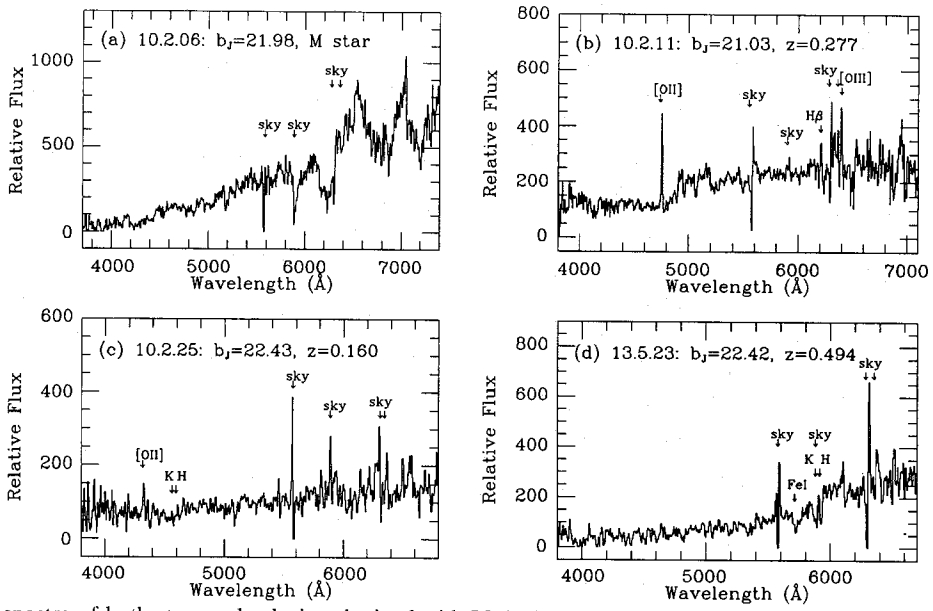

Figure 3. Example spectra of both stars and galaxies obtained with LDSS in this survey. Both emission and absorption-line objects can be identified even at the survey limit of $b_J = 22.5$.

Table 3. — *continued*

(1) ID (*f.z.#*)	(2) α (1950)	(3) δ (1950)	(4) b_J	(5) b_J-r_F	(6) S/G	(7) z	(8) Q	(9) W_λ (Å)
00.2.20	00 55 04.68	−27 47 25.5	21.82	—	g	0.000	5	—
00.2.21	00 54 53.15	−27 49 16.1	21.92	0.91	s	0.000	2	—
00.2.22	00 54 56.83	−27 43 44.5	22.00	2.50	s	0.000	1	—
00.2.23	00 54 54.36	−27 47 55.3	22.01	—	g	0.000	5	—
00.2.24	00 54 49.44	−27 45 40.3	22.02	0.74	g	0.225	2	30
00.2.25	00 54 57.21	−27 43 05.0	22.07	1.54	g	0.317	1	34
00.2.26	00 54 57.76	−27 44 09.0	22.10	1.43	s	0.333	1	28
00.2.27	00 54 53.92	−27 48 06.2	22.12	0.36	g	—	3	—
00.2.28	00 54 31.28	−27 43 28.6	22.13	—	s	0.000	5	—
00.2.29	00 55 05.38	−27 43 54.4	22.14	1.11	g	—	3	—
00.2.30	00 54 54.41	−27 42 19.4	22.15	1.76	g	—	3	—
00.2.31	00 54 46.93	−27 40 08.1	22.18	1.50	g	0.464	1	40
00.2.32	00 54 33.65	−27 46 09.1	22.22	1.63	s	0.213	1	—
00.2.33	00 54 51.03	−27 48 52.2	22.24	—	g	0.000	5	—
00.2.34	00 54 47.02	−27 42 05.2	22.28	1.76	g	—	3	—
00.2.35	00 54 56.54	−27 38 27.5	22.33	1.27	g	—	3	—
00.2.36	00 54 38.69	−27 48 42.2	22.34	1.34	g	—	4	—
00.2.37	00 54 48.97	−27 38 05.8	22.36	—	s	—	4	—
00.2.38	00 54 26.75	−27 50 05.2	22.38	0.37	g	—	4	—
00.2.39	00 54 52.18	−27 40 19.1	22.38	1.00	g	—	3	—
00.2.40	00 55 06.27	−27 38 42.6	22.38	1.40	s	—	4	—
00.2.41	00 54 48.39	−27 42 32.4	22.39	2.63	s	0.421	1	—
00.2.42	00 54 56.25	−27 44 35.7	22.40	—	g	0.563	2	10
00.2.43	00 54 44.23	−27 49 31.5	22.48	0.52	g	—	4	—
00.2.44	00 54 49.99	−27 48 16.6	22.51	0.71	g	—	4	—
00.2.45	00 55 01.33	−27 46 36.7	22.51	0.55	g	0.150	1	41
00.2.46	00 54 51.46	−27 47 12.7	22.53	—	g	0.000	5	—
00.2.47	00 54 53.88	−27 49 03.7	22.55	-0.44	g	—	4	—
00.2.48	00 54 54.97	−27 45 52.6	22.63	-0.19	g	0.176	2	16
00.2.49	00 54 51.79	−27 38 53.9	22.63	1.26	g	0.202	2	10
10.2.01	10 43 55.12	+00 10 04.1	21.03	1.12	s	0.266	1	26
10.2.02	10 43 48.77	+00 07 38.6	21.40	0.73	s	0.549	2	8
10.2.03	10 43 51.47	+00 04 26.5	21.49	0.34	s	0.319	1	8
10.2.04	10 43 55.81	+00 08 50.6	21.71	0.58	s	0.543	2	—
10.2.05	10 44 02.86	+00 00 58.5	21.72	1.91	s	0.303	1	4
10.2.06	10 44 04.87	+00 06 55.2	21.98	2.16	s	0.000	1	—
10.2.07	10 43 57.41	+00 03 37.7	22.10	0.28	s	—	3	—
10.2.08	10 43 53.08	+00 03 54.7	22.19	2.41	s	0.000	1	—
10.2.09	10 43 52.07	+00 02 47.8	22.22	2.15	s	0.000	1	—
10.2.10	10 43 46.53	+00 04 57.7	22.26	1.35	s	—	3	—
10.2.11	10 44 01.25	+00 09 41.5	21.03	1.24	g	0.277	1	27
10.2.12	10 44 05.59	+00 05 20.6	21.13	1.62	g	0.168	1	10
10.2.13	10 43 53.15	+00 02 24.3	21.38	1.81	g	0.437	1	5
10.2.14	10 43 59.00	−00 00 05.7	21.47	1.70	g	0.304	1	8
10.2.15	10 43 49.40	+00 08 11.9	21.70	1.77	g	0.451	1	8
10.2.16	10 44 00.69	+00 06 17.5	21.73	0.97	g	0.151	1	21
10.2.17	10 44 04.53	+00 00 18.3	21.75	1.26	g	0.302	1	37
10.2.18	10 43 55.30	+00 10 22.8	21.82	0.63	g	—	3	—
10.2.19	10 43 56.27	+00 05 48.9	21.99	1.33	g	0.179	1	16
10.2.20	10 43 45.16	+00 07 16.6	22.02	1.79	g	0.188	2	—
10.2.21	10 43 59.04	+00 11 34.5	22.03	0.69	g	—	4	—
10.2.22	10 43 49.11	+00 11 09.3	22.11	0.89	g	0.180	1	31
10.2.23	10 44 04.00	+00 01 53.1	22.36	1.29	g	0.665	2	75
10.2.24	10 43 47.59	+00 09 19.5	22.42	2.23	g	0.000	1	—
10.2.25	10 43 48.10	+00 06 38.0	22.43	0.90	g	0.160	1	20
10.2.26	10 43 53.62	+00 00 37.3	22.45	1.08	g	—	4	—
10.4.01	10 43 52.94	−00 09 24.0	21.60	2.12	s	0.000	1	—
10.4.02	10 43 46.82	−00 11 08.6	21.67	2.32	s	0.000	1	—
10.4.03	10 43 52.63	−00 00 59.2	21.74	0.72	s	—	3	—
10.4.04	10 43 48.52	−00 05 56.7	21.79	1.03	s	—	3	—
10.4.05	10 43 56.97	−00 12 07.9	21.80	2.19	s	0.000	1	—
10.4.06	10 43 47.34	−00 02 17.8	22.32	2.11	s	0.237	2	18
10.4.07	10 43 56.11	−00 10 46.8	22.47	1.57	s	0.000	2	—
10.4.08	10 43 54.47	−00 08 11.1	22.48	2.06	s	0.000	1	—
10.4.09	10 43 57.24	−00 05 28.1	20.99	1.11	g	0.000	1	—
10.4.10	10 43 59.11	−00 07 34.0	21.08	1.53	g	0.290	1	22
10.4.11	10 43 43.95	−00 08 56.8	21.14	1.12	g	0.263	1	46
10.4.12	10 44 00.02	−00 04 44.4	21.22	2.34	g	0.437	1	6
10.4.13	10 43 46.45	−00 06 40.5	21.25	0.71	g	0.148	1	42
10.4.14	10 43 57.70	−00 08 35.4	21.34	0.86	g	0.138	1	17
10.4.15	10 43 59.26	−00 06 19.4	21.67	1.77	g	0.394	1	14
10.4.16	10 43 53.30	−00 04 21.0	21.67	—	g	0.000	5	—
10.4.17	10 43 57.45	−00 01 59.8	21.73	1.25	g	0.191	1	22
10.4.18	10 43 55.44	−00 00 34.8	21.76	2.14	g	—	4	—
10.4.19	10 43 55.47	−00 09 54.7	21.98	1.26	g	0.029	2	38
10.4.20	10 43 53.95	−00 12 31.6	22.15	0.95	g	0.420	2	46
10.4.21	10 43 46.68	−00 11 38.6	22.21	0.79	g	0.527	2	31
10.4.22	10 43 44.75	−00 10 23.2	22.24	0.84	g	0.232	1	14
10.4.23	10 43 51.88	−00 01 33.4	22.40	2.79	g	—	3	—
10.4.24	10 43 48.91	−00 03 01.3	22.48	2.00	g	—	3	—
13.2.01	13 41 48.20	+00 11 35.1	21.59	2.17	s	0.198	2	28
13.2.02	13 41 59.22	+00 02 01.8	21.65	0.98	s	0.000	1	—
13.2.03	13 42 02.55	+00 04 55.7	21.67	—	s	0.000	1	—
13.2.04	13 42 04.91	+00 09 03.6	21.72	0.96	s	0.000	1	—
13.2.05	13 41 50.32	+00 00 27.3	21.95	2.17	s	—	4	—
13.2.06	13 41 57.03	+00 08 17.2	22.17	1.04	s	0.000	1	—
13.2.07	13 41 55.17	+00 07 26.5	21.61	1.24	g	0.325	1	45
13.2.08	13 41 56.91	+00 01 09.8	21.63	0.55	g	0.179	1	17
13.2.09	13 42 06.31	+00 06 49.2	21.69	1.41	g	0.386	1	59
13.2.10	13 42 04.80	+00 11 09.9	21.71	—	g	0.424	1	—
13.2.11	13 42 06.59	+00 01 34.2	21.72	—	g	—	3	—
13.2.12	13 42 05.17	+00 09 32.3	21.82	2.07	g	0.255	1	—
13.2.13	13 42 05.53	+00 10 26.5	21.82	1.92	g	0.430	1	23
13.2.14	13 42 05.85	+00 03 41.5	21.82	1.65	g	—	3	—
13.2.15	13 41 59.17	+00 04 10.7	21.98	1.87	g	—	3	—
13.2.16	13 41 49.54	+00 00 46.7	22.04	1.39	g	0.340	2	48
13.2.17	13 41 52.15	+00 03 07.1	22.08	1.42	g	—	3	—
13.2.18	13 42 07.04	+00 06 28.6	22.14	1.35	g	0.531	1	42
13.2.19	13 41 49.61	+00 02 49.7	22.10	1.51	g	—	3	—
13.2.20	13 41 48.26	+00 09 56.7	22.14	1.23	g	0.512	1	63
13.2.21	13 42 04.48	+00 02 27.7	22.16	1.55	g	0.385	1	38
13.2.22	13 42 06.40	+00 12 04.5	22.19	1.25	g	0.422	2	29
13.2.23	13 41 59.64	+00 05 42.9	22.33	1.49	g	—	3	—
13.4.01	13 41 02.32	−00 01 12.8	21.51	2.14	s	0.000	1	—
13.4.02	13 41 06.05	−00 02 50.8	21.63	0.75	s	0.127	1	88
13.4.03	13 41 15.63	−00 06 16.0	21.95	—	s	—	4	—
13.4.04	13 41 06.80	−00 05 19.0	22.02	0.30	s	—	3	—
13.4.05	13 41 14.21	+00 01 52.7	22.07	1.58	s	0.000	1	—
13.4.06	13 41 11.13	−00 02 32.7	22.13	0.63	s	0.000	2	—
13.4.07	13 41 11.70	−00 00 06.3	22.16	1.50	s	0.000	2	—
13.4.08	13 41 08.80	+00 03 25.1	22.32	1.09	s	0.000	2	—
13.4.09	13 41 00.45	−00 01 54.1	22.41	1.55	s	0.000	2	—
13.4.10	13 41 05.01	+00 01 14.8	21.31	1.32	g	0.361	1	39
13.4.11	13 41 05.52	+00 05 06.9	21.39	0.59	g	0.439	2	52
13.4.12	13 41 13.65	+00 02 21.5	21.50	—	g	0.120	1	38
13.4.13	13 41 16.57	−00 03 22.9	21.51	1.85	g	0.419	1	12
13.4.14	13 41 18.82	−00 03 54.4	21.54	1.45	g	0.273	1	17
13.4.15	13 41 09.10	+00 00 11.7	21.70	2.66	g	0.415	1	4
13.4.16	13 41 13.68	+00 00 31.2	21.72	0.95	g	0.120	1	56
13.4.17	13 41 14.10	−00 04 33.1	21.76	1.70	g	0.543	2	25
13.4.18	13 41 13.45	+00 03 51.6	21.96	1.43	g	—	3	—
13.4.19	13 41 12.83	+00 04 24.4	22.04	1.89	g	0.359	2	—
13.4.20	13 41 16.34	−00 00 49.3	22.07	1.80	g	0.437	1	4
13.4.21	13 41 19.74	−00 01 33.0	22.08	1.05	g	0.165	2	21
13.4.22	13 41 15.73	+00 00 51.9	22.10	0.67	g	0.086	2	36
13.4.23	13 41 12.15	−00 04 59.8	22.19	—	g	0.552	2	39
13.4.24	13 41 04.13	+00 03 03.4	22.21	2.82	g	—	3	—
13.5.01	13 41 05.62	+00 14 59.5	21.83	0.69	s	0.000	1	—
13.5.02	13 41 11.88	+00 15 20.3	22.03	2.28	s	0.000	1	—
13.5.03	13 41 12.83	+00 04 24.4	22.03	1.89	s	0.000	1	—
13.5.04	13 41 09.75	+00 15 49.0	22.13	1.03	s	0.000	2	—
13.5.05	13 41 02.61	+00 13 13.4	22.36	0.85	s	0.000	2	—
13.5.06	13 41 12.78	+00 08 06.0	22.40	1.25	s	0.112	2	54
13.5.07	13 41 13.60	+00 08 29.5	21.32	0.56	g	0.220	1	24
13.5.08	13 41 17.64	+00 11 00.6	21.45	0.53	g	—	3	—
13.5.09	13 41 14.56	+00 05 13.3	21.51	1.32	g	—	3	—
13.5.10	13 41 06.50	+00 12 19.8	21.57	1.45	g	0.329	1	31
13.5.11	13 41 18.93	+00 11 24.9	21.60	1.47	g	0.490	2	16
13.5.12	13 41 13.13	+00 11 45.5	21.63	1.19	g	0.678	2	27
13.5.13	13 41 10.16	+00 06 49.6	21.69	1.49	g	—	3	—
13.5.14	13 41 08.95	+00 12 52.5	21.83	—	g	0.255	1	29
13.5.15	13 41 13.08	+00 13 45.7	22.00	—	g	—	3	—
13.5.16	13 41 00.13	+00 10 42.0	22.01	1.77	g	0.000	1	—
13.5.17	13 41 16.42	+00 09 32.0	22.17	2.33	g	0.329	1	—
13.5.18	13 41 17.63	+00 14 27.7	22.22	1.86	g	—	3	—
13.5.19	13 41 07.92	+00 05 51.9	22.26	0.30	g	0.088	1	11
13.5.20	13 41 06.72	+00 09 01.8	22.30	1.75	g	0.521	1	25
13.5.21	13 41 08.37	+00 10 02.1	22.33	0.65	g	0.136	2	26
13.5.22	13 40 59.99	+00 14 06.1	22.42	2.53	g	—	3	—
13.5.23	13 41 02.25	+00 07 40.0	22.42	2.75	g	0.494	1	—

Notes: (i) the ID in column 1 is *f.z.#*, where *f* is the field R.A., *z* is the zone number and # is the object number within the zone; (ii) column 6 is the COSMOS star/galaxy classification; (iii) column 8 is the redshift quality class (see text); (iv) column 9 is the restframe equivalent width of [O II] 3727 Å.

few objects to be spurious. Such objects can be readily identified by comparing the photometric magnitude and a spectroscopic *slit* magnitude. This latter is determined on a relative scale by multiplying the flux-calibrated spectrum by the transmission function for the b_J passband. Although, as expected, stars and galaxies show differing relations between their slit and photometric magnitudes, the rms scatter in both relations is about 0.45 mag and is reasonably constant from field to field. All seven objects with $Q=5$ have very discrepant ($>3\sigma$) slit magnitudes, and none are detected in r_F. The 13 objects in the sample with $Q=4$ lie at the extreme north or south of zones, where a large fraction of each spectrum falls outside the undispersed field of view and so cannot be corrected for the severe distortion in the corners of the dispersed field.

The entire sample listed in Table 3 contains a total of 169 objects. Of these, 20 are classified $Q=4$ or 5 and can thus be excluded from further discussion without affecting the statistical properties of stars and galaxies in the catalogue. (The $Q=4$ objects are excluded on the basis of image processing difficulties and without consideration of possible features or signal-to-noise.) Of the remaining 149 objects in the survey for which spectra were obtained (i.e. $Q=1$, 2 or 3), 33 are spectroscopically identified as stars, 87 are galaxies with redshifts and 29 have no identifications. The overall success rate for identifications is thus 81 per cent, which is comparable to the success rate of 85 per cent obtained in the fibre survey of BES. If we adopt the COSMOS image classifications for the unidentified objects, we then obtain a success rate for galaxies alone of 78 per cent, similar to the overall rate. The incompleteness varies somewhat from field to field (*cf.* Table 2); due both to different weather conditions and the different mask strategy adopted as the project proceeded [for the first zone attempted (00.2), the minimum slit length adopted was somewhat smaller than optimum and consequently the incompleteness and loss of objects due to distortion problems is relatively high even with the long integration time].

5 THE REDSHIFT DISTRIBUTION

The galaxy redshift distributions for each of the three AAT plate fields are shown in Fig. 4. As expected, some clustering is apparent. The three fields are consistent, however, in that the redshift distributions peak in the range $0.2 \le z \le 0.4$ and reach an apparent cut-off at $z \approx 0.6$–0.7. The mean (field-weighted) redshift for the survey is $\bar{z} = 0.312 \pm 0.022$, where the error is determined from the field-to-field scatter (see Table 4). Before discussing the redshift distribution further, we need to understand the origins of the 19 per cent incompleteness in the spectroscopic identifications.

Fig. 5(a) shows the b_J magnitude distributions of the unidentified objects compared to the whole sample (excluding objects with $Q=4$ or 5). A K–S two-sample test implies that the b_J distributions of the $Q=1$ or 2 and $Q=3$ objects differ at the 5 per cent level, implying there does exist some bias with apparent magnitude. The fraction of objects without redshifts increases steadily across the magnitude ranges $b_J = 21$–21.5, 21.5–22 and 22–22.5, being 9, 16 and 27 per cent, respectively. For those also detected in r_F, the b_J–r_F distributions of identified and unidentified objects are, however,

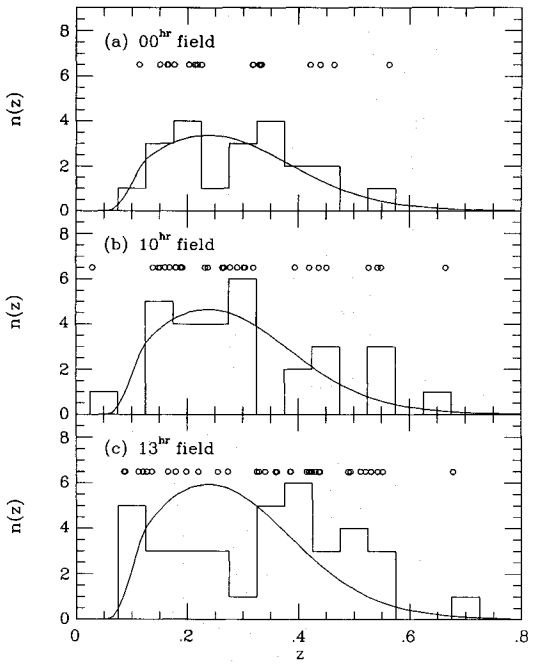

Figure 4. The redshift distributions for each of the three survey fields. The circles above each histogram mark the redshifts of the individual glaxies. Also shown is the prediction of the no-evolution model, appropriately normalized for each field.

Table 4. Mean redshifts and comparison with no-evolution model.

(1) Field	(2) N	(3) $\bar{z}$	(4) P_{KS}
00 hr	21	0.296	0.37
10 hr	29	0.302	0.74
13 hr	37	0.337	0.009
All	87	0.312	0.016

Notes: (i) P_{KS} is the confidence level at which the observed $n(z)$ is inconsistent with the NE $n(z)$.

indistinguishable under a similar K–S test (Fig. 5b). The fraction of objects with no r_F detection is no higher for the $Q=3$ objects (7 per cent) than for those with $Q=1$ or 2 (6 per cent). Apparent magnitude, but not colour, is thus correlated with the redshift incompleteness in the survey.

Is the increasing incompleteness with apparent magnitude simply due to poorer signal from fainter objects, or does it signify a population of high-redshift objects which present no clear identifying features within our observed spectral window? High-redshift galaxies will, in the main, lie at the faint end of the sample, so it is important to distinguish between these possibilities. Since [O II] 3727 Å should be detectable out to at least 6800 Å (i.e. $z \approx 0.82$), and is found in 85 per cent of the identified galaxy spectra, it seems unlikely that the survey incompleteness could result from difficulty in recognizing galaxies with redshifts $z > 0.6$. This argument may be quantified by computing the likelihood of seeing [O II] 3727 Å at redshifts beyond $z = 0.6$ in the following manner.

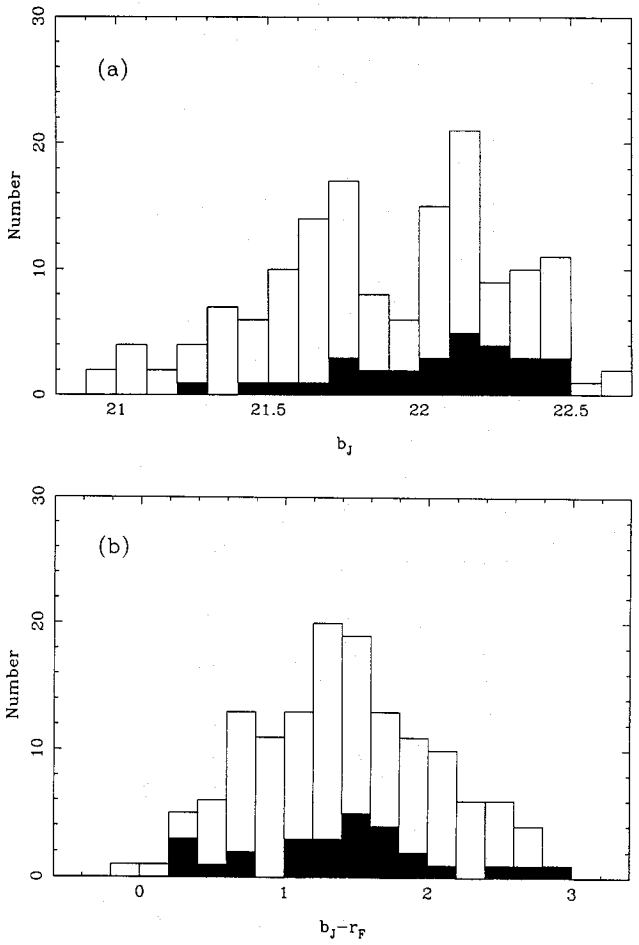

Figure 5. (a) The b_J distribution of unidentified ($Q=3$) objects (solid histogram) compared to that of both identified and unidentified objects ($Q=1,2,3$) (open histogram); (b) the same but for b_J-r_F.

The restframe equivalent widths of detected [O II] are given in column 9 of Table 3. Fig. 6 shows the relation between the signal-to-noise ratio (S/N) in the continuum adjacent to [O II] and the equivalent width of the detected line, which implies that [O II] is detectable if the signal-to-noise ratio in the line (calculated according to simple assumptions which, for an unresolved line with this observing set-up, give the approximate relation $S/N_{\rm line} \approx 0.4\, W_\lambda S/N_{\rm continuum}$) exceeds a threshold level of about 20. Given this threshold and a known S/N in the continuum over some wavelength range, we may compute the minimum equivalent width of [O II] that would be detectable in that range. The continuum S/N may be estimated directly and reliably for each observed spectrum, including those which remain unidentified, in the two sky-line-free windows 6000–6200 and 6600–6800 Å (corresponding to $z=0.61$–0.66 and $z=0.77$–0.82).

We thus estimate the minimum detectable equivalent width of [O II] in these windows for all 29 spectra of quality $Q=3$ for which no redshift could be obtained. Assuming that the distribution of equivalent widths at these higher redshifts is not too dissimilar from that actually observed at a lower mean redshift, we can compute the likelihood of detecting [O II] if the line were present in one of the two windows. The mean probability of detection for the 29 unidentified spectra

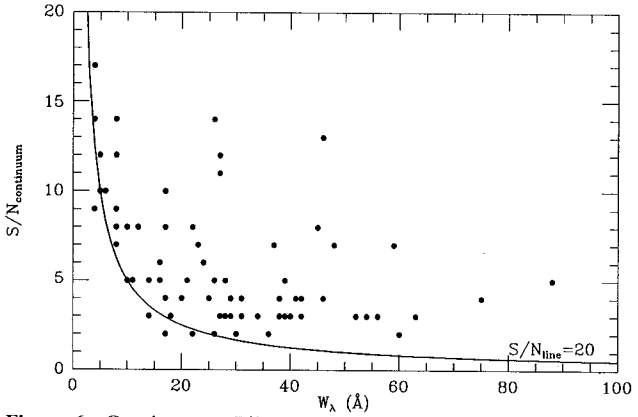

Figure 6. Continuum S/N ratio versus equivalent width for detected [O II] 3727 Å emission lines in the survey. Points above the smooth curve have a S/N ratio in the line of more than 20.

is 55 per cent, so we would have expected to recognize and obtain a redshift for about half of the unidentified galaxies *if they had had redshifts in one of these two windows.*

To determine the strength of the constraint implied by *not* finding *any* galaxies in these redshift ranges, we need to make some assumption about the form of the redshift distribution beyond $z=0.6$. Without invoking particular physical models, we can estimate the likely fraction of objects in the two redshift windows using the plausible assumptions that any hypothetical high-z tail to $n(z)$ joins smoothly on to the observed $n(z)$ at $z=0.6$ and thereafter decreases monotonically. For simplicity, we ignore for the moment the possibility that $n(z)$ is bimodal, with a second peak at higher redshifts. As an example of a truncated tail we adopt a simple linear decline, and as an example of a more extended tail we adopt an exponential decline. Fixing the scalelengths and normalizations of these tails using the above constraints, we find that 26 per cent of galaxies in the linear tail, and 23 per cent of galaxies in the exponential tail, would have redshifts such that [O II] would be in the sky-line-free windows. We conclude that the fraction of galaxies in these windows is only weakly dependent on the form of $n(z)$, and for plausible extensions of $n(z)$ to higher redshifts has a value ~ 0.25.

To summarize: we would have expected to have been able to identify 55 per cent of our unidentified objects if they have redshifts in either of two redshift ranges between $z=0.6$ and $z=0.8$; plausible extensions of the redshift distribution imply that 25 per cent of galaxies in any monotonically declining redshift tail lie in these ranges, so we might have expected to identify $0.25\times 0.55\times 29 \simeq 4$. The Poisson probability of finding none when four are expected is only 2 per cent, so this is good evidence that the unidentified galaxies do not form an extension of the observed $n(z)$ to higher redshifts. Although clustering will modify the significance of this result, its effects are reduced since we are combining three independent fields. We conclude that the survey incompleteness is due to the difficulty of recognizing weak features in spectra with the S/N ratios obtained here, and that the increase in incompleteness with apparent magnitude is due to worsening S/N.

The redshift distribution of all the survey galaxies is shown in Fig. 7(a). The redshift distribution for the range $20\le b_J\le 22.5$, obtained by combining the results of this survey with those of BES, is given in Fig. 7(b). This information is presented in an alternative form in Fig. 8, which shows

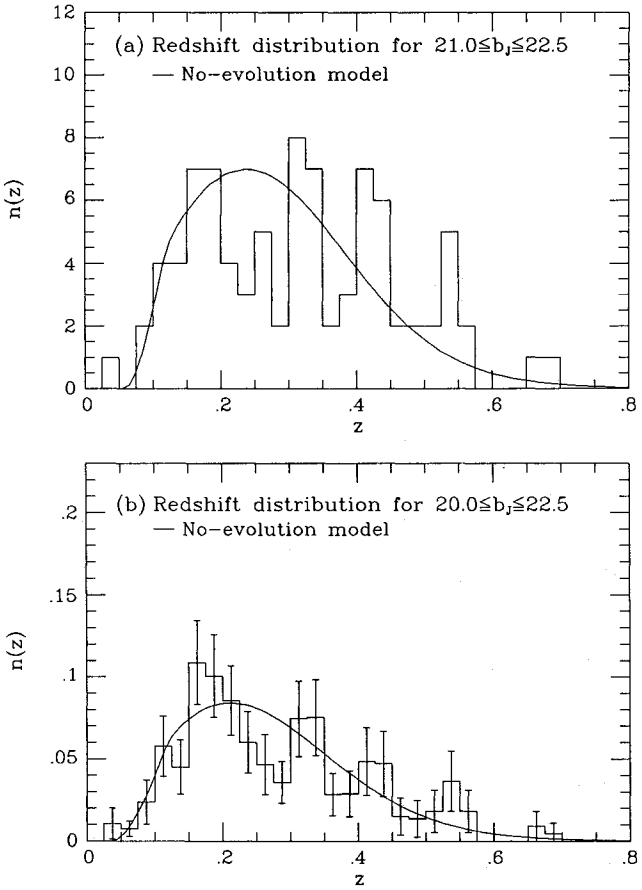

Figure 7. (a) The redshift distribution for the whole survey. The line is the no-evolution model prediction; (b) the combined redshift distribution for this survey and that of BES, normalized so that $\int n(z)\,dz = 1$. The line corresponds to the no-evolution model.

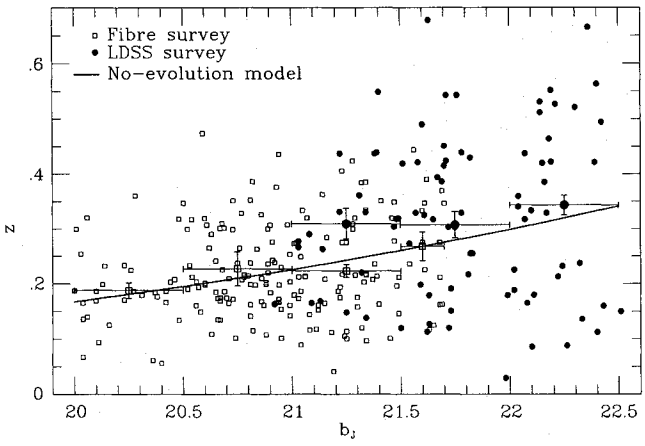

Figure 8. Redshift versus apparent magnitude for this survey (filled circles) and BES (open squares). The mean redshifts in various magnitude intervals (points with error bars) are compared to the predictions of the no-evolution model (solid line).

the distribution of redshift as a function of apparent magnitude, with the mean redshift (and its field-to-field variation) indicated in various magnitude intervals (with widths indicated by the horizontal bars). The trend of $\bar{z}(m)$ is consistent across the full magnitude range spanned by the two surveys. [Note that because of the small correction to the photometric zeropoint in the SGP field (Section 3), the BES survey actually reaches to $b_J = 21.71$ in that one field.]

6 DISCUSSION

6.1 The form of the redshift distribution

Despite the fact that it fails to predict the number counts, a non-evolving model provides a useful baseline with which to compare the observed redshift distributions. The no-evolution (NE) model we employ here is identical to that described by BES. The local galaxy properties, specifically the luminosity function parameters and relative numbers of different morphological types, are based on the Durham/Anglo-Australian redshift survey (DARS: Peterson *et al.* 1986). *K*-corrections are taken from King & Ellis (1985). Further details of the NE model are discussed by BES. In particular, we note that predictions based on luminosity functions parameterized by optical/infrared b_J–K colours, reflecting more accurately the energy distributions used to calculate the various *K*-corrections, lead to near-identical predictions. The model used here assumes $q_0 = 0.5$; assuming other values leads to changes in the predicted $n(z)$ which are insignificant compared to the effects of other uncertainties in the model.

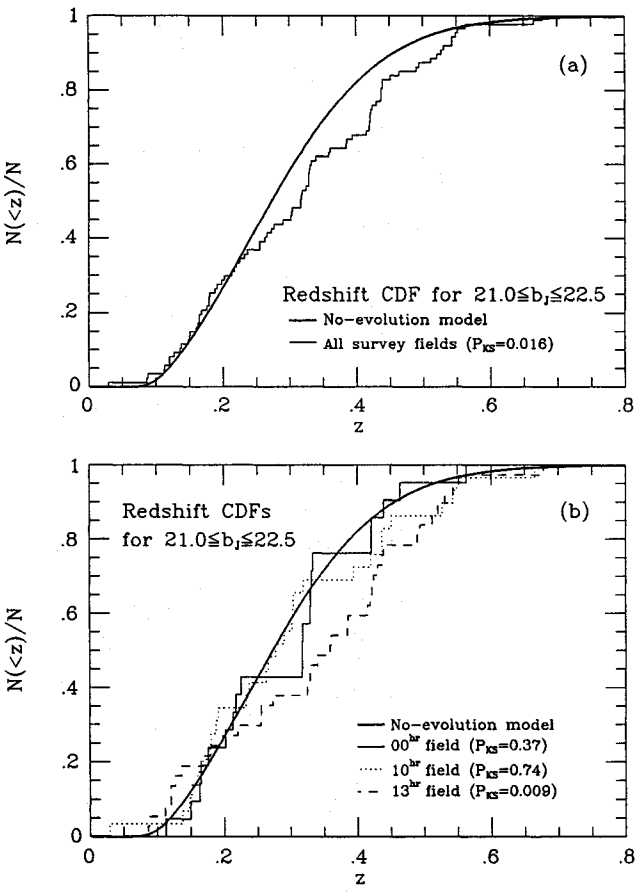

Figure 9. (a) Comparison of observed redshift distribution with no-evolution model via a one-sample K–S test; (b) the same, but for each individual survey field.

Neglecting the effects of clustering on the redshift distribution, we may test whether the observed $n(z)$ is consistent with a model $n(z)$ via a one-sample K–S test. Such a test shows that the redshift distribution for the entire survey is inconsistent with the NE distribution at the 1.6 per cent confidence level (see Fig. 9a). However, dividing the sample by fields and re-applying the same test, we find that the 00- and 10-hr fields are both reasonably consistent with the NE model (see Table 4 and Fig. 9b), and that the effect is largely due to galaxies in the 13-hr field (see Fig. 4c). This implies that deviations from the NE model are, most likely, explicable in terms of clustering in the 13-hr field, although conceivably the other two fields could be anomalous in which case some mild evolution might be consistent with the data. Further data are needed to clarify this. (Note that there is no evidence to suggest that the three fields could not have a common underlying redshift distribution; K–S *two*-sample tests comparing $n(z)$ for the pairs of fields 00 hr/10 hr, 00 hr/13 hr and 10 hr/13 hr only find them inconsistent at the 56, 17 and 8 per cent confidence levels, respectively.)

The most significant aspect of the comparison relates to the *form* of $n(z)$, which shows no significant high or low redshift excess compared to the NE prediction. Using the arguments of Section 5 to rule out a missed high-redshift tail to $n(z)$, we are able to extend to a new faint limit of $b_J = 22.5$, and a mean redshift of $\bar{z} = 0.31$, the result found by BES: the excess galaxies apparent in the number counts have the same range of redshifts [and the same $\bar{z}(m)$ – see Fig. 8] as we would expect for a non-evolving galaxy population possessing the properties found in local surveys. In fact, since the NE model predicts only about half the observed number of galaxies in the magnitude range covered by the survey, we can conclude that *even if* all 29 unidentified objects are galaxies in a missed high redshift tail (contrary to the arguments of the previous section), *nonetheless* 50 per cent of the galaxies making up this excess must *still* be in the observed redshift range. Thus, regardless of what is happening at high redshift, this survey demonstrates that at least half of the evolution leading to the excess in the number counts to $b_J = 22.5$ occurs at redshifts less than $z \approx 0.5$.

A quantitative and model-independent upper limit for the fraction of galaxies brighter than $b_J = 22.5$ which are at redshifts higher than the observed z_{max} (≈ 0.7) may be established as follows. If some hypothetical model predicts that a fraction p of galaxies brighter than $b_J = 22.5$ are at $z > z_{max}$, then the fact that no such galaxies were found would allow the model to be ruled out at the $\alpha = (1-p)^N$ confidence level, where N is the observed number of galaxies. Conversely, we can rule out at the α confidence level more than a fraction $p = 1 - \alpha^{1/N}$ of galaxies brighter than $b_J = 22.5$ having $z > z_{max}$. Since all 87 identified galaxies have $z < 0.7$, we may infer that the fraction of galaxies brighter than $b_J = 22.5$ with $z > 0.7$ is less than 5.2 per cent at the 1 per cent confidence level, or less than 2.6 per cent at the 10 per cent confidence level. While these limits are quite low, in practice they only apply to galaxies at redshifts lower than the highest redshift at which [O II] 3727 Å is readily recognized ($z \approx 0.8$).

It is important here to stress two points. First, by the nature of the discussion above, the surveys are useful in constraining evolution where the effects are luminosity-independent and monotonically increasing with redshift in such a way as to reproduce the counts. It may be possible to reconcile certain mild evolutionary models with the $n(m, z)$ data discussed here (*cf.* Koo 1986), although as BES showed it is important to compare model predictions with the spectra of typical excess galaxies and not simply the joint $n(m, z,$ colour) data. Secondly, our discussion of incompleteness does not account for the possibility that $n(z)$ is bimodal, as might be the case if galaxies underwent some spectacular phase at high z. Since at least half of the excess has $z < 0.5$, this solution could be considered somewhat contrived, though we discuss it further in Section 6.3.

How much luminosity evolution at $z \sim 1.5$–2.5 is therefore allowed by the results of our redshift survey? If, relaxing the cautious approach we have thus far taken, we assume that *none* of the $b_J \leq 22.5$ galaxies has $z > 0.7$, and we examine the hypothesis originally proposed on the basis of the photometric studies (e.g. Koo 1981; Ellis 1982) that there exist blue luminous galaxies in the redshift interval $1 < z < 2$ whose star-formation rate has since rapidly declined, we can calculate the amount of luminosity evolution compatible with their non-appearance to our magnitude limit of $b_J = 22.5$. We adopt the UV–optical SED of NGC 4449 (Bruzual & Ellis, unpublished) to compute the effects of the K-correction. This is a nearby low-luminosity galaxy with very blue colours ($U-B = -0.25$, $B-V = 0.38$) exemplary of the intense star-formation inferred for the faint galaxies providing much of the excess count population.

In the absence of *any* luminosity evolution, such a galaxy at M* is bright enough to be selected in our sample to $z \approx 0.8$, up to which redshift [O II] 3727 Å should be readily detected. At $z \sim 1.5$ (where C IV 1549 Å and Mg II 2798 Å should both be detectable), such a star-forming galaxy would be visible at $b_J = 22.5$ with an additional 1.2 mag of luminosity evolution if $q_0 = 0.5$, and 1.8 mag if $q_0 = 0.1$. These constraints are actually quite significant because they refer to the brightening at a rest wavelength of $\lambda_{b_J}/(1+z) \approx 1800$ Å, where there is strong sensitivity to any decline in the star formation rate.

Complex models with numerous formation redshifts or star formation histories for different spectral classes are not necessary to see the significance of such a limit on the past brightening of M* galaxies. If we first consider single burst (c-) models successful in reproducing the SEDs of present day ellipticals (Bruzual 1984), we note that with $H_0 = 50$ km s^{-1} a formation redshift of $z \approx 2$–2.5 generates an object whose rest-frame UBV colours at $z \approx 1.5$ are remarkably similar to NGC 4449 (and so to the faint population observed). However, in the absence of further star formation, the decline in 1800 Å flux since $z = 1.5$ is much larger than the 1–2 magnitudes necessary to bring such galaxies within our survey magnitude limit. Luminous ellipticals therefore cannot have formed in this way since $z \approx 2.5$, for otherwise their precursors at $z \approx 1.5$ would be readily visible in our redshift samples.

Less straightforwardly, we can place some limits on the past evolution of spirals. To match the present-day colours of intermediate spirals, many authors have realized the need to maintain a near-constant star formation rate with time. However, such a star formation history predicts little evolution in colour or luminosity. We can explore the extent to which such galaxies *might* have been brighter at $z \sim 2$ (thereby contributing to the count excess) in the context of our redshift survey. We apply bursts of varying strengths at $z \approx 2.5$ to a

galaxy already undergoing a long-term phase of constant star-formation. To generate objects as blue as NGC 4449 at $z \sim 2$ we find a strong burst is needed, consuming at least as much gas as that consumed during the quiescent lifetime. In this case the UV flux declines dramatically to the present day. Although the effect is not so dramatic, again it appears that *luminous* spirals could not have attained such a blue colour at $z \sim 1.5$–2 and maintained their present SEDs without being much more luminous and hence visible in the LDSS survey.

Thus any recent evolution at the bright end of the luminosity function must have been small *for all classes of galaxy*, otherwise high-redshift objects would have been detected in this survey to $b_J = 22.5$. A full analysis, comparing the numbers expected with the completeness limits achieved with LDSS, is beyond the scope of this paper, particularly in view of BES' suggestion that evolution is luminosity-dependent with unknown fractions undergoing bursts. However, since the above discussion applies to M* galaxies, any such population would not be insignificant in our volumes. Although our conclusions are weakened for low q_0 cosmologies, particularly in the case of spiral galaxies, continuity arguments suggest that the blue excess seen to $b_J \sim 24$ is more likely due to the precursors of lower luminosity objects at moderate redshifts (as postulated by BES) or to a new population at redshifts $z > 2$ (a possibility we take up in Section 6.3). Only further spectroscopic surveys will allow this ambiguity to be resolved.

6.2 The distribution of [O II] equivalent widths

Thus far we have emphasized the lack of any direct evidence for galaxy evolution in the form of the redshift distribution, inferring from this and the steep slope of the number counts some conclusions about the form this evolution must take. As BES have noted, however, the equivalent width, W_λ, of the [O II] emission line at 3727 Å can be used as an indicator of the degree of star formation activity. In their survey to $b_J = 21.5$, they found about double the number of galaxies with $W_\lambda \geq 20$ Å that would be expected on the basis of a non-evolving population having the properties (specifically, the correlation between W_λ and $b_J - K$) found in the local DARS galaxies. Noting that this excess represented a fraction of the galaxy population comparable to the number count excess, they suggested identifying the additional large-W_λ galaxies with the evolving population revealed by the counts.

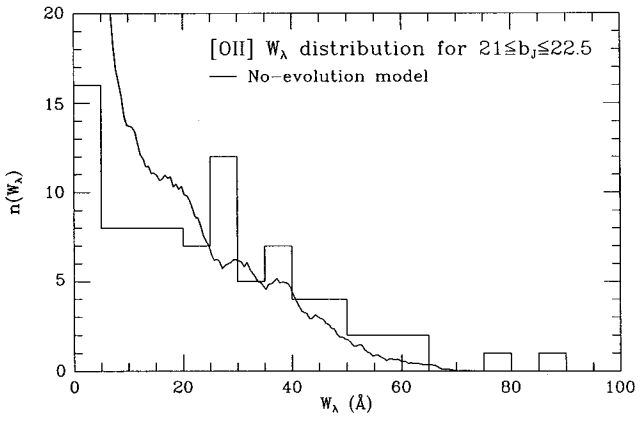

Figure 10. The histogram of [O II] 3727 Å equivalent widths for the 87 identified galaxies with $21 \leq b_J \leq 22.5$. The curve is the NE model prediction, normalized assuming all 29 unidentified objects are galaxies (i.e. to a total sample size of 116).

Fig. 10 shows the distribution of rest-frame [O II] 3727 Å equivalent widths for the 87 galaxies in this survey. Also shown is the predicted distribution of W_λ in this magnitude range for a non-evolving population. This NE model has been normalized assuming all 29 unidentified objects are in fact galaxies (i.e. to a total sample size of 116). This is clearly an upper limit to the normalization. Nonetheless, it is seen that the observed number of galaxies with $W_\lambda \geq 20$ Å is in excess of the model by > 40 per cent. There is no evidence that the redshift distribution of these $W_\lambda \geq 20$ Å galaxies differs significantly from those with $W_\lambda < 20$ Å or from the prediction of the NE model.

Although this result confirms the excess of galaxies with large equivalent widths found by BES, the size of this excess is less than that of the excess in the number counts and, if anything, is less biased to high values than in the $20 \leq b_J \leq 21.5$ sample. There appears, therefore, to be some conflict with BES' identification of the excess counts with these strong W_λ galaxies. In comparison with BES, however, there are several difficulties of interpretation. Apart from the fact that the new sample is only half as large, the measured W_λ also have larger errors (~ 5–10 Å) due to the fainter continuum and the lower dispersion used in this survey. Aperture effects, on the other hand, are unlikely to be significant: with LDSS the typical effective area is 1.7×2.5 arcsec at $\bar{z} = 0.31$, compared with a fibre diameter of 2.7 arcsec at $\bar{z} = 0.22$. We note finally that Koo (1989), using a multislit approach similar to LDSS for a large, though less deep, sample, also finds a substantial excess of galaxies with strong [O II] 3727 Å emission lines.

6.3 Flat-spectrum galaxies

Tyson (1988) and Cowie *et al.* (1988) have recently noted a substantial population of very faint ($R > 23$), flat-spectrum ($B-V \approx 0.2$, $V-I \approx 0.8$) objects which may be galaxies in the midst of a strong and early burst of star formation. Although the redshift of $z = 3.4$ claimed for one such galaxy by Cowie & Lilly (1989) has now been withdrawn (Cowie & Lilly 1990), the average surface brightness on the sky of flat-spectrum objects suggests that, *regardless of their redshifts*, they have contributed a significant fraction (probably > 20 per cent) of the metals in the Universe (Cowie 1988). These results make it of interest to examine more closely the bluest objects in the present sample.

All but six of the 87 identified galaxies and two of the 29 unidentified objects in this survey have $b_J - r_F$ colours. The $b_J - r_F$ distribution for the identified galaxies is shown in Fig. 11, together with the distribution of all objects with $21 \leq b_J \leq 22.5$ in the six LDSS zones which were classified as galaxies by COSMOS. These two distributions are consistent under a two-sample K–S test, as expected. Both are also in good agreement with the results of Metcalfe *et al.* (1987) for the same magnitude range, and show a similar excess of blue galaxies with respect to the predictions of the NE model (see Fig. 11; note that the models are normalized to the observed

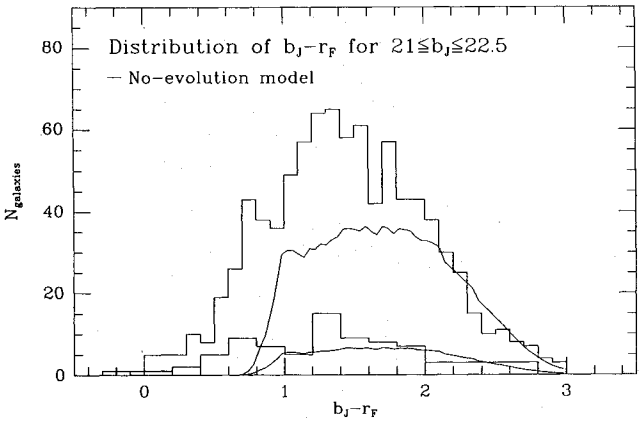

Figure 11. The b_J-r_F distributions and NE model predictions in the range $21\leq b_J\leq 22.5$ for (i) all COSMOS-classified galaxies in the six LDSS zones (upper histogram and curve); (ii) 81 survey galaxies with spectroscopic identifications (lower histogram and curve). The models are normalized to the number of galaxies with $b_J-r_F\geq 2$ (see text for details).

number of galaxies with $b_J-r_F\geq 2.0$, as such galaxies cannot have evolved over the range of redshifts found in the survey). Despite the large excess of galaxies with $b_J-r_F\leq 1.6$, the range of observed colours is, with the possible exception of the very bluest, consistent with that expected for non-evolving galaxies at the observed redshifts. This is demonstrated in Fig. 12, which plots b_J-r_F against redshift for 81 survey galaxies in comparison to the unevolved colours of various galaxy types as a function of redshift (based on K-corrections from King & Ellis 1985).

There are seven survey objects with $Q=1$–3 that have $b_J-r_F<0.5$, and it is interesting to consider these in light of the abovementioned claims of a new blue population at faint limits. There are four *identified* galaxies with $b_J-r_F<0.5$ (Fig. 12). All four have redshifts $z<0.4$, and one (10.2.03) has precise CCD colours ($B-R=0.48$, $R-I=0.49$) which place it firmly in the flat-spectrum category. From the three *unidentified* objects with $b_J-r_F<0.5$, and the total survey area (0.109 deg^{-2}) and sampling rate (26 per cent), we obtain an upper limit of 100 deg^{-2} for the surface density of possible *high-redshift* flat-spectrum galaxies with $21<b_J<22.5$. In

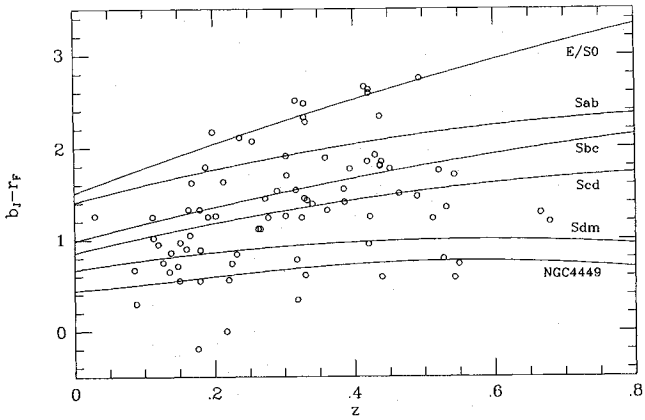

Figure 12. The distribution of b_J-r_F with redshift for 81 survey galaxies. The curves are the unevolved colours as a function of redshift for various galaxy types.

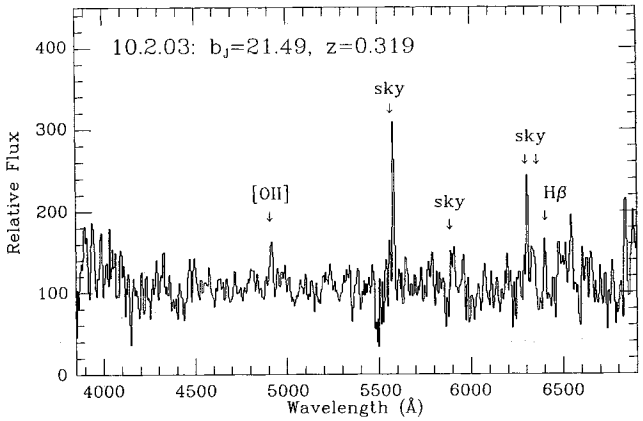

Figure 13. Spectrum of the relatively bright ($b_J=21.49$) $z=0.319$ galaxy 10.2.03, whose CCD colours classify it as a flat-spectrum galaxy according to the criteria of Cowie *et al.* (1988).

the range $23<I<24$ (corresponding to $24<B<25$), Cowie & Lilly report a surface density of $\sim 10^4$ deg^{-2} for flat-spectrum objects. If, as Cowie & Lilly claim, these are high-redshift galaxies, the surface density of high-redshift flat-spectrum galaxies increases by a factor of at least 100 over this 2.5 mag interval. This increase corresponds to a $n(m)$ slope of 0.8 or more, implying either extraordinary evolution or the onset of an altogether new population.

The fact that all four *identified* galaxies with $b_J-r_F<0.5$ are at low redshifts, however, suggests a more likely interpretation is that the Cowie *et al.* objects are a faint extension of these blue low-redshift galaxies to moderate ($z<1$) redshifts rather than a new high-redshift population. Examination of the LDSS spectrum of 10.2.03 (Fig. 13) shows weak [O II] and Hβ at $z=0.319$. It is conceivable that a poorer signal-to-noise spectrum of such a galaxy at a fainter limit might be mistaken for that of a high-redshift galaxy. If we assume that all seven objects with $b_J-r_F<0.5$ are indeed at low redshift, we obtain a surface density of 250 deg^{-2} for *low-redshift* flat-spectrum galaxies with $21\leq b_J\leq 22.5$. Over the 2.5 mag interval to the Cowie & Lilly sample, this corresponds to a $n(m)$ slope for this population of $0.64^{+0.21}_{-0.05}$. In a non-evolving model, even a population of galaxies with SEDs as blue as that of NGC 4449 only has a $n(m)$ slope of 0.42. Evolution at the faint end of these galaxies' luminosity function would therefore be necessary if *all* the Cowie *et al.* objects are to be explained as a faint extension of the observed population of blue low-redshift galaxies. Further spectroscopy of these faint, flat-spectrum galaxies will be necessary to establish the redshift domain and evolutionary significance of this population.

6.4 Compact objects

The decision, for reasons of completeness, not to employ morphological classification techniques for star/galaxy separation when selecting samples for this survey means that we are able to judge the effectiveness of such techniques. We may also determine whether morphologically selected samples are neglecting important populations of compact extragalactic objects.

Because (semi)-automated algorithms for star/galaxy separation are now commonly used in obtaining number

Table 5. Comparison of COSMOS image classification with spectroscopic identifications.

		COSMOS class		
		star	gal	
Spectral	star	20%	3%	⇒ 13% stars misclassified galaxies
class	galaxy	9%	49%	⇒ 16% galaxies misclassified stars
	no ID	3%	16%	

counts of both stars and galaxies, a spectroscopic check on the accuracy of one such method (that implemented on the COSMOS machine) provides an important guide to the extent of the biases these algorithms may introduce. Table 5 summarizes this comparison. For these deep AAT plates, and neglecting the objects without spectral identifications, the COSMOS algorithm correctly classifies 85 per cent of objects in the range $21 \leq b_J \leq 22.5$, with about 15 per cent of both stars and galaxies misclassified as the other. Of the objects with no spectroscopic identification, 84 per cent were classified galaxies by COSMOS. This is in comparison to the 64 per cent with identifications which COSMOS classified as galaxies, and reflects the relative ease of spectroscopically identifying faint stars (usually M-type, with strong spectral features) compared to galaxies.

The COSMOS classification leads to undercounting the galaxies by about 5 per cent. This error is small in comparison to the fractional excess of galaxies in the number counts at these magnitudes, and, though systematic, would tend to minimize the size of the observed excess. It is comparable to other possible sources of systematic error in the number counts. For example, an error of this amplitude corresponds to over-estimating the magnitude zeropoint by 0.05 mag.

No unusual population of compact extragalactic objects was discovered amongst the spectroscopically-identified galaxies that COSMOS classified as stars. Amongst the 14 objects that fall into this category, there is a slight tendency toward red $b_J - r_F$ colours and weak or absent [O II]. The redshift distribution is, however, consistent with those of the galaxies which were classed as such by COSMOS. Since only 3 per cent of the survey sample were classified as stars by COSMOS but had no spectral identification, compact extragalactic objects must be at least this rare. No QSOs were found in the survey.

The properties of the stars found in this survey will be discussed in a future paper dealing with a spectroscopic survey to $b_J = 23.5$ of compact objects.

7 CONCLUSIONS

We may summarize the main conclusions of this survey as follows:

(i) Using a new multislit spectrograph, LDSS, we have increased the limiting magnitude of field redshift surveys by ~ 1.0 mag over previous work whilst maintaining a high degree of completeness. Our survey of randomly-selected objects with $21.0 \leq b_J \leq 22.5$, chosen regardless of image classification, has allowed us to address the origin of the significant excess of field galaxies found photometrically at these limits.

(ii) Our observed redshift distribution, which spans the range $z = 0.0$–0.7, matches closely that predicted by a no-evolution model based on local galaxy properties *despite the factor of 2 shortfall in predicted counts at this limit.* From considerations of the signal-to-noise ratio in emission-line detections, we demonstrate that our incompleteness (amounting to ~ 19 per cent) *cannot* significantly distort the observed $n(z)$ out to $z \sim 0.8$, and that *at least* half the extra galaxies seen in the counts must have $z < 0.5$.

(iii) We also find, in comparison with a no-evolution model, a significant excess (40 per cent) in the number of galaxies with [O II] 3727 Å equivalent widths greater than 20 Å. This supports Broadhurst *et al.*'s hypothesis that there is increased star formation in low-luminosity galaxies at moderate redshifts. The excess observed is not increasing significantly at fainter limits, and so the strong-lined galaxies do not appear, by themselves, to fully account for the excess observed in the counts.

(iv) The absence of *any* identified galaxies with $z > 0.7$ to $b_J = 22.5$ places important constraints on the evolution of luminous galaxies since $z \sim 1.5$–2, although a larger, statistically complete, survey to this depth is required to make precise statements. General luminosity evolution of the form once expected to provide the bulk of the steep count slope to $b_J = 24$ must be less than ~ 1.5–2.0 mag over this period.

(v) We have identified a number of blue (in $b_J - r_F$), low-redshift galaxies, similar in colour to the *flat-spectrum* objects claimed by Cowie & Lilly (1989) to be a new high-redshift population emerging beyond $b_J \sim 24$. We find only marginal evidence for a steeper than average increase in the surface density of such objects from our survey to the deep CCD limits. Whether these flat-spectrum galaxies are simply an extension to moderate redshifts of the star-forming sub-M* population identified in the redshift surveys or a genuine high-redshift population requires further statistically complete spectroscopy at limits comparable to, or just beyond, that achieved here.

ACKNOWLEDGMENTS

We acknowledge the generous allocations of time on the Anglo-Australian Telescope which made this work possible. The photographic photometry was performed on the COSMOS machine at the Royal Observatory, Edinburgh, and calibrated with CCD data kindly supplied by Laurence Jones (Durham) and Lance Miller & Karl Glazebrook (ROE). Further CCD photometry was obtained at Kitt Peak National Observatory, which is run by AURA. We thank Tom Broadhurst, Laurence Jones, Nigel Metcalfe, Tom Shanks and David Koo for useful discussions. All the computing was carried out on the Durham node of STARLINK. MMC was supported by a SERC PDRA.

REFERENCES

Boyle, B., 1986. *PhD thesis,* University of Durham.
Boyle, B. J., Shanks, T., Fong, R. & Peterson, B. A., 1987. *Mon. Not. R. astr. Soc.*, **227,** 717.
Broadhurst, T. J., Ellis, R. S. & Shanks, T., 1988. *Mon. Not. R. astr. Soc.*, **235,** 827.
Bruzual, G., 1983. *Astrophys. J.*, **273,** 105.

Bruzual, G., 1984. In: *Spectral Evolution of Galaxies,* Rutherford Appleton Laboratory, RAL-008.
Colless, M. M. & Hewett, P. C., 1987. *Mon. Not. R. astr. Soc.,* **224,** 453.
Colless, M. M., Ellis, R. S. & Taylor, K., 1988. In: *The Epoch of Galaxy Formation,* p. 359, eds Frenk, C. S., Ellis, R. S., Shanks, T., Peacock, J. A. & Heavens, A., Kluwer, Dordrecht.
Couch, W. J. & Sharples, R. M., 1987. *Mon. Not. R. astr. Soc.,* **229,** 423.
Couch, W. J., Shanks, T. & Pence, W. D., 1985. *Mon. Not. R. astr. Soc.,* **213,** 215.
Cowie, L. L., 1988. In: *The Epoch of Galaxy Formation,* p. 31, eds Frenk, C. S., Ellis, R. S., Shanks, T., Peacock, J. A. & Heavens, A., Kluwer, Dordrecht.
Cowie, L. L. & Lilly, S. J., 1989. *Astrophys. J.,* **336,** L41.
Cowie, L. L. & Lilly, S. J., 1990. In: *The Hubble Symposium: The Evolution of the Universe of Galaxies,* ed. Kron, R., Astr. Soc. Pacif. Conference Series, in press.
Cowie, L. L., Lilly, S. J., Gardner, J. & McLean, I. S., 1988. *Astrophys. J.,* **332,** L29.
Dressler, A. & Gunn, J. E., 1982. *Astrophys. J.,* **263,** 533.
Ellis, R. S., 1980. *Phil. Trans. R. Soc. Lond. A,* **296,** 355.
Ellis, R. S., 1982. In: *The Origin and Evolution of Galaxies,* p. 255, eds Jones, B. J. & Jones, J. E., Reidel, Dordrecht.
Ellis, R. S., 1987. In: *Instrumentation for Cosmology,* p. 57, ed. Davies, R. L., NOAO, Tucson.
Ellis, R. S. & Parry, I. R., 1988. In: *Instrumentation for Ground-Based Optical Astronomy, Proc. of 9th Santa Cruz Summer Workshop,* p. 192, ed. Robinson, L., Springer, New York.
Godwin, J. G., 1976. *PhD thesis,* University of Oxford.
Gray, P. M., 1986. *Proc. Soc. photo-opt. Instr. Eng.,* **627,** 96.
Hall, P. & Mackay, C. D., 1984. *Mon. Not. R. astr. Soc.,* **210,** 979.
King, C. R. & Ellis, R. S., 1985. *Astrophys. J.,* **288,** 456.
Koo, D. C., 1981. *PhD thesis,* University of California.
Koo, D. C., 1986. *Astrophys. J.,* **311,** 651.
Koo, D. C., 1988. In: *The Epoch of Galaxy Formation,* p. 71, eds Frenk, C. S., Ellis, R. S., Shanks, T., Peacock, J. A. & Heavens, A., Kluwer, Dordrecht.
Koo, D. C. & Kron, R., 1988. In: *Towards Understanding Galaxies at High Redshift,* p. 209, eds Kron, R. & Renzini, A., Kluwer, Dordrecht.
Koo, D. C. & Szalay, A. S., 1984. *Astrophys. J.,* **282,** 390.
Kron, R. G., 1978. *PhD thesis,* University of California, Berkeley.
Kron, R. G., 1982. *Vistas Astr.,* **26,** 37.
MacGillivray, H. T. & Stobie, R., 1984. *Vistas Astr.,* **27,** 433.
Majewski, S. R., 1988. In: *The Epoch of Galaxy Formation,* p. 85, eds Frenk, C. S., Ellis, R. S., Shanks, T., Peacock, J. A. & Heavens, A., Kluwer, Dordrecht.
Metcalfe, N., Fong, R., Jones, L. R. & Shanks, T., 1987. In: *High Redshift and Primeval Galaxies,* p. 37, eds Bergeron, J. *et al.,* Editions Frontières, Gif sur Yvette, France.
Oke, J. B., 1974. *Astrophys. J. Suppl.,* **27,** 21.
Peterson, B. A., Ellis, R. S., Kibblewhite, E. J., Bridgeland, M. T., Hooley, T. & Horne, D., 1979. *Astrophys. J.,* **233,** L109.
Peterson, B. A., Ellis, R. S., Bean, A. J., Efstathiou, G., Shanks, T., Fong, R. & Zou, Z.-L., 1986. *Mon. Not. R. astr. Soc.,* **221,** 233.
Shanks, T., Stevenson, P. R. F., Fong, R. & MacGillivray, H. T., 1984. *Mon. Not. R. astr. Soc.,* **206,** 767.
Sharples. R. M., Ellis, R. S. & Gray, P. M., 1988. *Mon. Not. R. astr. Soc.,* **231,** 479.
Stevenson, P. R. F., Shanks, T., Fong, R. & MacGillivray, H. T., 1985. *Mon. Not. R. astr. Soc.,* **213,** 953.
Tyson, J. A., 1988. *Astr. J.,* **96,** 1.
Tyson, J. A. & Jarvis, J. F., 1979. *Astrophys. J.,* **230,** L153.
Wynne, C. G. & Worswick, S. P., 1988. *Observatory,* **108,** 161.